[1]
Manuscript prepared for J. Name
with version 2015/04/24 7.83 Copernicus papers of the LaTeX class copernicus.cls.
Date: 28 October 2015

Multi-model ensemble analysis of Pacific and Atlantic SST variability in unperturbed climate simulations

D. Zanchettin[1,2], O. Bothe[1,3], A. Rubino[2], and J. H. Jungclaus[1]

[1]Max Planck Institute for Meteorology, The Ocean In The Earth System, Bundesstrasse 53, 20146 Hamburg, Germany
[2]University of Venice, Calle Larga Santa Marta, Dorsoduro 2137, Venice, Italy
[3]formerly at: Leibniz-Institute for Atmospheric Physics at the University of Rostock, Schlossstrasse 6, 18225 Kühlungsborn, Germany

Correspondence to: D. Zanchettin (davide.zanchettin@mpimet.mpg.de)

Abstract. We assess internally-generated climate variability expressed by a multi-model ensemble of unperturbed climate simulations. We focus on basin-scale annual-average sea-surface temperatures (SSTs) from twenty multicentennial pre-industrial control simulations contributing to the fifth phase of the Coupled Model Intercomparison Project (CMIP5). Ensemble spatial patterns of regional modes of variability and ensemble (cross-)wavelet-based phase-frequency diagrams of corresponding paired indices summarize the ensemble characteristics of inter-basin and regional-to-global SST interactions on a broad range of timescales. Results reveal that tropical and North Pacific SSTs are a source of simulated interannual global SST variability. The North Atlantic-average SST fluctuates in rough co-phase with the global-average SST on multidecadal timescales, which makes it difficult to discern the Atlantic-Multidecadal-Variability (AMV) signal from the global signal. The two leading modes of tropical and North Pacific SST variability converge towards co-phase in the multi-model ensemble, indicating that the Pacific Decadal Oscillation (PDO) results from a combination of tropical and extra-tropical processes. No robust inter- or multi-decadal inter-basin SST interaction arises from our ensemble analysis between the Pacific and Atlantic oceans, though specific phase-locked fluctuations occur between Pacific and Atlantic modes of SST variability in individual simulations and/or periods within individual simulations. The multidecadal modulation of PDO by the AMV identified in observations appears to be a recurrent but not typical feature of ensemble-simulated internal variability. Understanding the mechanism(s) and circumstances favoring such inter-basin SST phasing and related uncertainties in their simulated representation could help constraining uncertainty in decadal climate predictions.

[1]The final publication of this manuscript is available at Springer via http://dx.doi.org/10.1007/s00382-015-2889-2. The current version differs from the published version in minor clarifying revisions of the text.

1 Introduction

Despite the extensive use of Coupled General Circulation Models (CGCMs) and Earth System Models (ESMs) important aspects of inter- and multi-decadal climate dynamics and variability remain poorly understood (Liu, 2012). Consider, for instance, the Atlantic Multidecadal Variability (AMV), which describes aspects of the low-frequency behavior of North Atlantic sea-surface temperatures (SSTs): Although numerical simulations identified the AMV as a feature of coupled ocean-atmosphere dynamics in the North Atlantic ocean more than one decade ago (e.g., Griffies and Bryan, 1997), climate simulations still show limits in the representation of observed AMV features (e.g., Kavvada et al., 2013), and the debate is still unsettled about the nature — internal rather than predominantly forced — of the 20th century AMV evolution (e.g., Knight, 2009; Medhaug and Furevik, 2011; Booth et al., 2012; Zanchettin et al., 2013; Zhang et al., 2013). Another example is the inter-basin relation between dominant modes of low-frequency SST variability in the Pacific and Atlantic oceans. The observed Pacific Decadal Oscillation (PDO) and the AMV appears to be strongly interrelated (d'Orgeville and Peltier, 2007; Zhang and Delworth, 2007; Wu et al., 2011), whereas the two phenomena can be identified as separate modes in long CGCM integrations (e.g., Park and Latif, 2010). Furthermore, compared to observations, coupled climate models are still affected by considerable biases in regional SSTs especially in the North Atlantic ocean that are associated, in the Northern Hemisphere, to cold biases resembling the Northern Hemisphere's annular mode (Wang et al., 2014). Temporally limited and spatially sparse observations, differently designed numerical experiments and structural model uncertainty impede firm conclusions about the mechanisms underlying inter- and multi-decadal climate variability. This study is concerned with the detection of robust low-frequency internally-generated variability in coupled climate simulations. We use a large multi-model ensemble of pre-industrial control climate simulations to assess dominant features of unperturbed basin-scale SST variability, and discuss implications for the interpretation of observed features.

Multi-model ensemble approaches reduce the peculiarities of individual simulations and/or deficiencies of individual models by combining the information into a multi-model "consensus" (in the ambit of weather forecasting see, e.g., Fritsch et al., 2000). Large multi-model collections of simulations contributing to coordinated intercomparison projects ('ensembles of opportunity') represent the most valuable tool to assess accuracy and robustness of climate features as they are simulated by state-of-the-art CGCMs and ESMs (e.g. Knutti et al., 2010). The largest ensembles of opportunity are provided by the fifth phase of the Coupled Model Intercomparison Project (CMIP5, Taylor et al., 2011) and the third phase of the Paleoclimate Modelling Intercomparison Project (PPMIP3, Braconnot et al., 2012). The performances of the CMIP5/PMIP3 multi-model ensemble has been assessed for the historical period (e.g., Bhend and Whetton, 2013; Joetzjer et al., 2013; van Oldenborgh et al., 2013) and within the paleo-context of the last millennium (Bothe et al., 2013).

Uncertainty in the estimates from the CMIP5/PMIP3 simulations stems at least partly from the high complexity of modern CGCMs and ESMs, which include increasingly extensive implementations of resolved and parameterized physics, e.g., cloud-microphysics (Andrews et al., 2012), and biogeochemical processes. Internal climate variability is an additional source of spread of ensemble-simulated climate trajectories. The imprint of applied forcings and ongoing internal variability on the climate system is unique, so that differences arise in simulated regional climate patterns and temporal evolutions from individual realizations within a forced single-model ensemble (Deser et al., 2012; Zanchettin et al., 2013, 2014). Therefore, there is need to comprehensively assess the internal climate dynamics and associated variability within a multi-model context in order to constrain our confidence on the explanation (prior to prediction) of natural climate phenomena and their simulated representation.

This study considers an ensemble based on multicentennial and millennial piControl simulations from the CMIP5/PMIP3 archive to assess whether robust features characterize state-of-the-art CGCMs and ESMs that point to a consistent description of the general dynamics behind internal climate variability. We explore regions and timescales that are of critical importance for the verification of 20th century historical simulations and for decadal climate predictability. We accordingly concentrate on Pacific and Atlantic SSTs as paramount conveyors of integrated interannual to multidecadal-to-centennial climate signals, and interpret the associated properties as representative of simulated coupled atmosphere-ocean physics. Our interpretation of the ensemble is based on a weak definition of multi-model consensus. We expect ambiguity to be a dominant property of the ensemble-simulated variability due to differences between individual ensemble members and inherent non-stationarity of simulated climate variability.

Our assessment focuses on within-ensemble robustness of spatial patterns of regional annual-average SST variability and emerging prevalent features of (cross-)wavelet-based phase-frequency diagrams of corresponding paired indices. We discuss our ensemble results in the light of analog results from observational data and previous hypotheses about low-frequency Pacific-Atlantic SST interactions.

2 Data and methods

2.1 Data

We use the 1870–2012 HadISST 1.1 monthly average SST dataset (Rayner et al., 2003) as our reference for the observational period. The dataset serves to introduce the methods, as reference for the model-ensemble results and to characterize the results in the light of known modes of SST variability. Therefore, we also use the following observational time series: the 1856–present monthly Nino3.4 time series and the unsmoothed monthly time series of the Atlantic Multidecadal Oscillation (AMO Enfield et al., 2001) index calculated at NOAA/ESRL/PSD1 from, respectively, the HadISST dataset and the Kaplan SST V2 dataset; the 1900–present monthly PDO index (Mantua et al., 1997) time series calculated at JISAO, Washington, from the UKMO Historical and Reynold's Optimally Interpolated SST datasets. Pre-processing of HadISST data includes removal of the local quadratic polynomial trend component.

We use the CMIP5 piControl simulations listed in Table 1, which describe unperturbed climates under pre-industrial, constant boundary conditions. Different simulations from the same model family are considered (ACCESS, CSIRO, GISS, GFDL, MPI-ESM), if the model configurations are different. For instance, the versions 1-0 and 1-3 of ACCESS differ for the included land component (MOSES and CABLE, respectively). MPI-ESM-P and -MR share the same atmospheric and ocean models, but in different resolutions, and differ in the inclusion of a dynamical vegetation component (Jungclaus et al., 2013; Giorgetta et al., 2013). Models from the GFDL family share the same atmospheric circulation model (AM3) but differ in the implemented physics and biogeochemistry of the ocean models. CESM1-BGC is an extension of CCSM4, sharing the same physical and land surface components but including the sea-ice model CICE4 (Long et al., 2013).

The piControl simulations often suffer from long-term drifts in the ocean state, likely due to an insufficient spin-up of the integration. A preliminary screening on global-average SST (GSST) time series allowed to eliminate, in some simulations, initial integration periods whose inclusion would have led to higher-order trends over the full period. Thus, pre-processing of SST data includes removal of the local long-term trend if a trend is found in the GSST (Table 1). Further pre-processing includes regridding of MPI-ESM-P/-MR data to a regular $1^\circ \times 1^\circ$ grid. The simulations in our ensemble have different durations, ranging from about 500 years to about 1000 years (Table 1). We therefore opt for non-uniform simulation lengths for our main analysis but also discuss the case of a 500-year homogenized ensemble.

The piControl simulations are generally tuned and run on similar but not the same mean climate states. The mean climate state can crucially influence simulated regional SST variability and associated teleconnections on both interannual (e.g., Müller and Roeckner, 2008; Choi et al., 2011) and inter- and multi-decadal (e.g., Yoshimori et al., 2010; Zanchettin et al., 2013) timescales. According to a preliminary assessment of GSST climatologies (results not shown), global climates in individual simulations generally do not differ substantially in terms of distribution and variability. GSST slightly differs in its average but features similar higher order moments and similar theoretical background spectra for most simulations. Only two models/simulations stand out: GISS-E2-H, with GSST ~ 1.1K warmer with weaker variance than the average of other simulations, and GFDL-CM3, with GSST slightly warmer with stronger variance.

Additionally, the 3100-year unperturbed simulation performed with the COSMOS-Mill version of the Max-Planck-Institute ESM (Jungclaus et al., 2010) is used because of its extraordinary length, which allows assessing the stationarity of multidecadal-to-centennial SST variability and inter-basin SST interactions in a full-complexity ESM over a multi-millennial period. MPI-ESM-COSMOS-

Mill is an older generation model compared to those included in our main ensemble and does not contribute to CMIP5/PMIP3. So, for the sake of clarity, the associated results are mostly presented in the supplementary material.

2.2 Methods

There are numerous indices in the literature describing Pacific and Atlantic SST variability (e.g., Liu, 2012), which may capture different aspects of regional SST variability and of inter-basin interactions. Our selection entails two linearly-independent indices for the Pacific and one index for the Atlantic, following those by Zhang and Delworth (2007). PAC1 and PAC2 are defined as, respectively, the first and the second principal component of annual-average SSTs over the tropical and North Pacific (120–240°E; 20S–50°N); ATL is the spatially-averaged annual-average SST over the North Atlantic (80°W–0; 0–60°N). We exclude regions strongly affected by sea-ice variability, such as the interior of the Labrador Sea (as in Zanchettin et al., 2014). Principal components are evaluated using an area-weighted covariance matrix. The sign of the principal components is chosen as to have a consistent signature within the ensemble and in observations over key regions: PAC1 indices are imposed to have a positive signature over the tropical Pacific; PAC2 indices are imposed to have a negative signature over the North Pacific Current region.

A comparative assessment of each index's spatial pattern in observations and individual simulations allowed excluding simulations poorly representing the observed pattern. Specifically, a simulation is excluded for analysis involving a given index, if the centers are largely displaced compared to observations or the spatial correlation between simulated and observed regression patterns is below 0.5 for that index (correlation is calculated over the index's domain defined above). Spatial correlations are calculated on the HadISST grid ($1^\circ \times 1^\circ$), requiring simulated data to be regridded accordingly via bilinear interpolation.

For the MPI-ESM-COSMOS-Mill simulation an Atlantic Meridional Overturning Circulation (AMOC) index is defined as the zonally-integrated meridional streamfunction in the Atlantic Ocean at 30°N and 1000 m depth. An Arctic Oscillation (AO) index is also defined for this simulation as the first principal component of winter (DJF) 500 hPa geopotential heights in the Northern Hemisphere, north of 20°N.

Cross-wavelet analysis (Grinsted et al., 2004) is performed for each individual simulation across all possible pairs of indices and GSST (Morlet, $\omega_0 = 6$). For each pair, relative phases are calculated locally in the time-frequency space as the argument of the complex cross-wavelet transform $W^{XY} = W^X W^{Y^*}$, where W^X is the wavelet transform of the first index and W^{Y^*} is the complex conjugate of the wavelet transform of the second index (Grinsted et al., 2004). We focus on periods characterized by strong variability within selected timescales in at least one of the paired indices, and therefore consider only significant regions of the cross-wavelet spectrum. Significance is calculated following Grinsted et al. (2004). Our analysis concerns three timescales: interannual (3 to 7 years), interdecadal (20 to 50 years), and multidecadal (50 to 90 years). Practically, we proceed as follows for each pair of indices and each considered timescale: significant (95% confidence) cross-wavelet phases resolved in the cross-wavelet domain are retained from all the individual simulations and merged in one ensemble-phase population for the considered timescale. Regions of the domain affected by borders are excluded. The empirical probability distribution of the so-merged ensemble phases is evaluated for 24 bins in the range $(-\pi+\pi/24, +\pi+\pi/24]$, where 0 indicates co-phase and $\pm\pi$ anti-phase. The phase-frequency diagram is then created by plotting the average cross-wavelet phases of each bin and the associated relative occurrences (i.e., frequencies) on polar coordinates.

Analytical calculation of test statistics for wavelet quantities is often difficult (Ge, 2008). We follow three different approaches to test the hypothesis that a prevalent phase-relationship exists between paired indices: a chi-square goodness-of-fit test against a uniform distribution (method 1), and two non-parametric Monte-Carlo tests where the randomization consists either of generating random autocorrelated processes whose parameters are estimated from the original series (method 2) or of randomizing the phases of the Fourier transforms of the original series (method 3). In (1), the test is performed on phase probabilities composited at $\pi/6$ intervals corresponding to eleven degrees of freedom. In (2), the order is subjectively set to be equal to the lag for which the autocorrelation of the substituted original series falls below the threshold of $1/e$. Test (3) is similar to the phase-scrambling Fourier transform method (see, e.g., Zanchettin et al., 2008). In (2) and (3), 1000 random series are generated for each index and each simulation. The corresponding ensemble *epds* of the cross-wavelet phases are evaluated as for the original series. The distribution of 1000 maximum *epd* values serves to estimate the likelihood of a random occurrence of an obtained result for each index-pair and timescale. More specifically, the existence of a prevalent phase relationship between the original series within a given timescale is said not to be a chance feature with confidence c (in percent) if the associated occurrence exceeds, in its mean value, the percentile c of the maximum values of the randomized *epds*. We expect robust signals to pass all three significance tests and, additionally, to refer to a non-negligible part of the variability in order to avoid sampling-related bias issues. Therefore, we consider significant phase-frequency relations to be non-representative if they stem from only sporadic events: A relation is interpreted as representative within the considered frequency band if the ratio of the significant region of the spectrum (from which the phase-frequency diagram is calculated) with the total is larger than 0.05 (5%) and anyway not smaller than the average ratios calculated from the randomized ensembles created for methods 2 and 3 as described above.

3 Results

3.1 Observational SST patterns and variability

Observations provide context to our model-ensemble analysis. We perform the full analysis including calculation of indices and associated spatial patterns, calculation of phase-frequency diagrams and cross-correlation profiles on the HadISST dataset. We also compare the PAC and ATL indices to associated known dominant modes of SST variability.

PAC1 explains about half of observed (detrended) tropical and North Pacific annual-average SST variability; its temporal evolution is characterized by strong interannual fluctuations (Figure 1a). The PAC1 pattern (Figure 1b) is significant over extensive regions of the Pacific. It features strong positive regression coefficients spreading zonally from the equatorial west Pacific to the tropical east Pacific, a positive horse-shoe pattern that extends the tropical signature along the extra-tropical eastern boundary, and a center of extensive negative correlations located in the middle of the extra-tropical basin. The pattern also entails a dipolar signature over the tropical and subtropical western North Atlantic.

The main features of the PAC1 pattern are reminiscent of those described by El Niño-Southern Oscillation (ENSO) in the tropics and by the PDO in the extra-tropics, though the negative center in the latter is typically stronger compared to PAC1. Accordingly, PAC1 is practically indistinguishable from the Nino3.4 index (Figure 1a, $r_{1870-2012} = 0.943$, p<0.001 accounting for autocorrelation in the data) describing ENSO variability in central-Pacific equatorial SSTs. PAC1 also significantly correlates with the PDO index ($r_{1900-2012} = 0.711$, p<0.001).

PAC2 explains about one tenth of observed (detrended) tropical and North Pacific annual-average SST variability, and its temporal evolution displays prominent multidecadal fluctuations (Figure 1c). There are sudden transitions in the 1940s and in the mid-1970s that are commonly associated to the PDO (e.g., Mantua et al., 1997). The PAC2 pattern (Figure 1d) shows a strong negative signature along the Kuroshio-Oyashio Extension. This is found also in the typical PDO pattern, although the latter is surrounded by a belt of positive correlations in a horse-shoe shape along the eastern boundary, which is missing in the PAC2 pattern. PAC2 further entails a strong positive signature over the Pacific warm pool region and its surroundings, and a negative signature over the western tropical North Atlantic. PAC2 is significantly correlated with the PDO but the two indices share only about one-third of their total variability ($r_{1900-2012} = 0.525$, p<0.001), likely due to the different interannual component they resolve (the correlation rises to $r = 0.890$ for 11-year smoothed indices). These results agree with former indications that PAC2 describes a North Pacific multidecadal mode that is equivalent to the PDO if the ENSO projection is removed from the SST anomalies (Zhang and Delworth, 2007). Whereas PAC1 and PAC2 are linearly independent, correlation increases for their decadally smoothed series ($r_{1875-2007} = 0.570$, p=0.315) suggesting that PDO physics may not be fully captured by a single EOF mode (e.g., d'Orgeville and Peltier, 2007).

ATL explains about 40% of observed (detrended) North Atlantic annual-average SST variability, and its temporal and spatial characteristics closely trace, as expected, those of the AMO index: the temporal evolution of ATL is characterized by AMO-like multidecadal fluctuations (Figure 1a, $r_{1870-2012} = 0.951$, p<0.001); its average pattern entails a pan-basin signature over the North Atlantic, with large positive regression coefficients in the tropical North Atlantic extending north-eastward along the eastern boundary, and further spreading westwards along the mid-latitude band. Weaker signals are detected in regions affected by sea-ice variability and in the western subtropical gyre region. The ATL pattern over the Pacific entails positive correlations over the tropical North Pacific, west of the date line, and along the basin's coastal belt.

Overall, our indices capture the regional SST variability associated to known phenomena of the tropical/North Pacific and North Atlantic oceans. The agreement is near-total for PAC1-ENSO and ATL-AMV/AMO, whereas the association between PAC2 and PDO suffers from a different interannual component embedded in the annual time series.

3.2 Observational phase relationships

Phase-frequency diagrams should be interpreted as follows. Deviations of the phase-frequency curve from a circle centered in the axes' center indicate that a prevalent phase relationship is likely between the two indices. An eastward oriented curve (phase difference of 0) indicates prevalent co-phase between the two indices. Similarly, a westward oriented curve (phase difference of $-\pi$ or π) indicates prevalent anti-phase. A northward or southward oriented curve indicates that the two indices fluctuate mostly in quadrature. If positive correlation is expected, the first (second) index leads with increasing lag for curves oriented according to increasing anticlockwise (clockwise) angles with respect to the co-phase semiaxis. If the two indices anti-correlate, the first (second) index leads with increasing lag for curves oriented according to increasing anticlockwise (clockwise) angles with respect to the anti-phase semiaxis. Our interpretation of phase-frequency diagrams is always assisted by cross-correlation profiles from high-pass and low-pass filtered (11-year running mean) paired indices.

Previous PDO-AMO cross-correlations analyses (Zhang and Delworth, 2007; Wu et al., 2011) provide context to the observational PAC2-ATL phase relations identified here. We use these indices as an introductory example for the interpretation of the phase-frequency diagrams. Note that both studies referenced above use a convention on the sign of the PDO that is opposite to the usual definition, which we adopted here as well. Figure 2a,d illustrates the observed wavelet phase relations between PAC2 and ATL in the form of (a) phase differences in the cross-wavelet domain and of (d) the derived phase-frequency diagram. Corresponding cross-correlation profiles are reported in supplementary Figure S1. Only phases at interannual and interdecadal timescales are fully resolved and hence reported in Figure 2b-g due to the limited length of the observational data. According to the corresponding phase-frequency diagram (blue curve in Figure 2d), the PAC2-ATL phase relation at interannual timescales is rather variable and frequencies (shown in the radial axis) never reach the significant levels determined by the two randomization-based tests. The curve nonetheless points to a phase lag of $\sim -\pi/4$, suggesting that PAC2 often lags ATL by ∼4.5-10.5 months. The blue numbers on the bottom right of the panel indicate that this diagram is representative of about 6% of the resolved cross-wavelet domain. This is within the average values obtained from the surrogate series (numbers in brackets). Features of the phase-frequency diagram are seen as the prevalently yellow-bluish patches in the upper part of Figure 2a. Given the different interannual variability resolved by PAC2 and by the PDO index (Figure 1c) it is not surprising that this result diverges from the 1-year delay of AMO on the PDO characterizing the associated high-frequency cross-correlation profile presented by Wu et al. (2011). The PDO and ATL indices indeed fluctuate often, though not significantly, in rough quadrature with PDO leading ATL by $\sim$0.75-1.75 years according to their interannual phase-frequency diagram (not shown). This agrees with the estimate by Wu et al. (2011).

A similar reading of Figure 2b indicates that, at interannual timescales, PAC1 and PAC2 preferably fluctuate in rough quadrature, reflecting the indices' construction. This prevalent phase relation is a significant feature, since it passes all tests, and is representative ($\sim$15%). Phasing is consistently significant across all tests and representative also at interannual timescales between PAC1 and GSST (Figure 2e), with PAC1 preferably leading by $\sim \pi/6$ or 3-7 months, and between GSST and ATL (Figure 2g), with GSST preferably leading by a few months.

The green curve in the phase-frequency diagrams of Figure 2d summarizes the PAC2-ATL phase relations at interdecadal timescales. It exemplifies the caution which is due in the interpretation of low-frequency results from observational time series and demonstrates the reliability of our approach based on both, significance and representativeness of the results. Being not representative ($\sim$2%) and failing two of the significance tests despite the narrowness of the associated phase-frequency curve, the interdecadal PAC2-ATL phasing likely reflects more a sampling issue rather than a specific and robust phase-locking between the two indices. Inspection of phases across the full cross-wavelet spectrum (Figure 2a) clarifies that the phase-frequency diagram captures the marginal features of what is a significant multidecadal-scale relation. Phases in this significant region of the multidecadal spectrum are mostly affected by border effects, but they indicate that, above the 50-year period, ATL leads PAC2 in anti-phase by $\sim \pi/4$ or $\sim$10 years, with a tendency towards tighter anti-phase through time. With due caution in the interpretation of these results, they are compatible with former indications of a decadal-scale lead of the AMO over the PDO (d'Orgeville and Peltier, 2007; Zhang and Delworth, 2007; Wu et al., 2011). There are no robust interdecadal phase relations between all other paired indices (Figure 2).

In summary, observational data provide reliable indications about interannual phase relations, but, as expected, pose evident limits to our interpretation of low-frequency variability. The limited length of the time series hampers a robust assessment of interdecadal signals and only partially resolves multidecadal timescales.

3.3 Ensemble SST patterns and variability

Figure 3 illustrates the CMIP5 ensemble-average regression patterns for the different indices. For each index, the pattern is said to be robust at locations where the local correlation is statistically significant (accounting for autocorrelation) in all simulations. The pattern is said to be incoherent over regions where local regressions disagree the most, specifically where the ensemble standard deviation of local regressions is larger than 0.2. For each index, only simulations passing the spatial correlation check are included (see methods).

The ensemble PAC1 pattern (Figure 3a) is robust over extensive regions of the Pacific. It closely traces the observational pattern (Figure 1b) in its shape but features overall weaker amplitudes. Spatial correlations between patterns of individual simulations and observations are always above 0.75 (not shown), except for GFDL-ESM2G which has a slightly lower value (0.69). Therefore, the following PAC1 ensemble analysis includes all simulations. Ensemble standard deviations above 0.2 indicate that individual simulations can differ strongly in the representation of PAC1 in the Pacific warm pool region. The pattern is also incoherent along the line separating positive and negative correlations in the extra-tropics, i.e. in the shape rather than the magnitude of the horse-shoe pattern. PAC1 explains between 18.8 and 41.8% of tropical and North Pacific SST variability, indicating that in individual simulations this leading mode can either dominate the total variability, or explain only a minor fraction of it. There is no consensus signature of PAC1 over the North Atlantic, although the ensemble-mean pattern entails positive regressions greater than 0.2 over the tropical North Atlantic.

PAC2 explains between 10.5 and 20.2% of tropical and North Pacific SST variability in individual simulations. PAC2 can have, basin-wide, different representations in different simulations (individual patterns not shown), highlighting within-ensemble inconsistent separation of Pacific SST variability into different modes. Spatial correlations between PAC2 patterns in individual simulations and observations are generally poorer than for the other indices (not shown), and in several cases drop below the 0.5 threshold. Accordingly, we exclude from the following PAC2 ensemble analysis the CSIRO-Mk3-6-0/-Mk3L-1-2, FIO-ESM, GISS-E2-H/-R and MIROC5. The reduced-ensemble PAC2 pattern (Figure 3b) entails strong and robust negative correlations along the Kuroshio-Oyashio Extension. Compared to the observational pattern (Figure 1d), this negative center is more zonally elongated with a somehow clearer surrounding belt of positive correlations (which are only locally robust). The horse-shoe pattern is weaker in PAC2 compared to PAC1 and does not connect to the equatorial Pacific anomaly, supporting the extra-tropical character of this mode. Ensemble standard deviations are extensively larger than 0.2, indicating that despite exclusion of some models, within-ensemble differences remain large. The PAC2 pattern indicates no consensus signature over the North Atlantic.

The ensemble ATL average pattern (Figure 3c) features an extensive and robust positive signature over the North Atlantic with a maximum in the tropics. The ensemble-simulated pattern agrees well with observations (Figure 1f) with spatial correlations between individual simulations and observations always above 0.9 (not shown), but with an overall weaker imprint. The strength of local regressions in the south-eastern branch of the subpolar gyre are about half of those in the tropics. This comparison with observations suggests that the AMV signature may be amplified under externally-forced conditions, especially in the tropics (Zanchettin et al., 2014). ATL explains between 15.5 and 27.6% of total variance of North Atlantic SST variability, which is smaller than for the observations (Figure 1e). The ATL pattern over the Pacific entails a positive though rather weak and locally incoherent imprint in eastern and central near-equatorial SSTs, which only partly agrees with the observed pattern. The ensemble-average pattern does not show the observed ATL signature over the western tropical North Pacific.

In summary, the spatial patterns of PAC1 and ATL are robust in the ensemble of unperturbed CMIP5/PMIP3 simulations over extensive regions. They overall compare well with the corresponding observed patterns, despite a generally weaker signature which we interpret as mainly a consequence of the overall weaker climate variability under unperturbed conditions. Furthermore, ATL and PAC1 signatures partly superpose in the tropical region, though not with consensus between simulations, suggesting that common variability may result from (lag-0) inter-basin interactions. Conversely, individual simulations differ in the variability captured by the PAC2 index and its ensemble robustness is more regionally confined. This required excluding some simulations to obtain a more consistent ensemble and ensemble relations comparable to the observational counterpart.

Details of the spectral features of the SST indices can vary strongly between simulations, also between those pertaining to the same family of models as shown, e.g., by CSIRO and GFDL simulations (Figure 4). There are, however, also features pointing towards general ensemble similarities. PAC1 expresses generally strong interannual variability, with different amplitude and characteristic frequency of the spectral peak(s) in the different models, and generally weak multidecadal and centennial variability. PAC2 generally exhibits more broadband variability, with comparatively stronger and often significant spectral amplitudes at multidecadal and longer timescales. ATL entails significant multidecadal and/or centennial variability in most but not all simulations. It additionally either presents strong PAC1-like interannual variability, or represents a process that is clearly redder than PAC1 and PAC2. The dominance of the interannual variability represents a potential major obstacle for our assessment of ensemble phase relations at inter- and multi-decadal timescales. In order to highlight the lower-frequency components, the following ensemble phase-frequency analysis for inter- and multi-decadal bands is first conducted for the original annual-average indices, and it is then repeated for decadally-smoothed (11-year running-mean) annual-average indices.

3.4 Ensemble phase relationships

On interannual timescales PAC1 and PAC2 fluctuate in rough quadrature (Figure 5a), as in observations (Figure 2b). There are significant and representative interannual phase relations between ATL and PAC1 (with phase difference of $\sim \pi/3$, Figure 5b), in close agreement with indications from observations (Figure 2c), and between ATL and PAC2 ($\sim -\pi/3$, Figure 5c). The ensemble PAC2-ATL phase-lag is mostly a consequence of the more representative phase lags governing the relation between each of these two indices and PAC1 (compare Figures 6a,b and 6c). We therefore do not interpret it as representing a one-way coupling between Atlantic and Pacific SSTs.

Ensemble interannual phase relations between GSST and the regional SST indices (Figure 6a-c) supported by cross-correlation analysis allow the following interpretation. PAC1 leads GSST by 1.5-3.5 months (Figure 6a), and this phasing is representative for more than 20% of the resolved cross-wavelet domain. PAC2 leads GSST in anti-phase (Figure 6b), with a larger phase difference of 0.5-1.2 years compared to PAC1. It is not clear whether this result is a consequence of the PAC1-PAC2 and PAC1-GSST phase lags rather than representing a dynamical interannual relation between extra-tropical North Pacific and global SSTs that is independent on PAC1/ENSO. Nonetheless, tropical and North Pacific SSTs clearly emerge as a source of interannual GSST variability. The ATL-GSST interannual phase distribution indicates a lagged dependency of ATL on GSST similar, in strength and representativeness, to the ATL-PAC1 relation (compare Figures 5b and 6c). This similarity prevents firm statements about whether ATL responds to an integrated global signal on these timescales rather than to a direct solicitation from Pacific SSTs.

In summary, the interannual model-ensemble results are in general agreement with indications from observations, with Atlantic and global signals lagging Pacific signals (compare blue curves in Figures 2, 5 and 6).

A rough, significant but non-representative (<5%) co-phase characterizes the PAC1-PAC2 inter- and multi-decadal variability as expressed by the annual indices (green and red curves in Figure 5a). Decadally-smoothed indices produce a highly representative (>40%) interdecadal phase-frequency curve confirming the significance of the rough co-phase. Thus PAC1 is a leading variable at these timescales (green curve in Figure 5d). Decadally-smoothed data further suggest that such a leading role of PAC1 on PAC2 could be extended to multidecadal variability (red curve in Figure 5d).

No robust prevalent interdecadal phase relations are detected between PAC1/PAC2 and ATL (green curves in Figure 5b,c,e,f). In decadally-smoothed data (Figure 5e,f) both PAC-ATL phase-frequency curves fail the uniformity test at interdecadal time scales, as the green curves only slightly deviate from the circle describing the uniform distribution. By contrast, there are at least hints of a multidecadal connection between PAC indices and ATL that support direction and timing of the observational low-frequency AMO-PDO connection (d'Orgeville and Peltier, 2007; Zhang and Delworth, 2007; Wu et al., 2011). These hints are the $\sim -\pi/2$ PAC1-ATL phasing from decadally-smoothed data implying that ATL preferably leads PAC1 by $\sim$12.5 years for a wavelet period of 50 years (Figure 5e), and the $2\pi/3$ PAC2-ATL phasing from annual data (Figure 5c) implying that ATL leads PAC2 in anti-phase by $\sim$8-15 years. The robustness of the diagnosed relations remains doubtful due to either weak significance or weak representativeness of the phase-frequency diagram in annual and decadally-smoothed data and, in the first place, due to the weak low-frequency variability of PAC1 (Figure 4). The cross-correlation profiles for low-pass filtered data in individual simulations further show the general weakness and great within-ensemble variability in the low-frequency PAC1/PAC2-ATL relation compared to observations (Figure S1). Hence, there is no clear regional driver of inter-basin multidecadal variability among our indices, but evidently there are periods in individual simulations when inter-basin SST fluctuations are characterized by a preferred phasing.

Using annual data, no robust features characterize inter- and multi-decadal phase relations between PAC1/PAC2 and GSST (Figure 6a,b). Robustness increases using decadally-smoothed data: a rough co-phase becomes apparent between PAC1 and GSST at interdecadal timescales and GSST often leads at multidecadal timescales (Figure 6d). The inter- and multi-decadal PAC2-GSST phase-frequency curves become highly representative and still indicate no preferred phasing due to failure of the uniformity test (Figure 6e). A broadband rough co-phase characterizes the ATL connection with GSST on inter- and multi-decadal timescales (Figure 5c,f). Representativeness is questionable only for the interdecadal time scale and annual data. The multidecadal phase-frequency ellipsoid's main axis is noticeably shifted clockwise from the co-phase semiaxis, implying that ATL signals are generally a consequent regional expression of global change. As previously discussed by, e.g., Grossmann and Klotzbach (2009) and Zanchettin et al. (2014), these results once more indicate that discerning the AMV signal from the global signal warrants careful attention.

3.5 Intrinsic variability

Non-stationarity of climate variability is an inherent feature of climate simulations (e.g., Zanchettin et al., 2010, 2013; Russell and Gnanadesikan, 2014). The multi-millennial control integration performed with the MPI-ESM-COSMOS-Mill model (Jungclaus et al., 2010) allows assessing the relation between intrinsic non-stationarity of inter- and multi-decadal SST variability and inter-basin SST interactions. Results for three subsequent 1000-year sub-periods (reported in the supplement) confirm the multi-model ensemble results. Specifically: Despite local differences, the regional SST patterns remain robust throughout the integration while the variability of the associated indices changes substantially (Figure S2). Differences in the spectral features between millennial sub-periods are negligible in the interannual band but spectral peaks in the multidecadal-to-centennial band differ in both, their amplitude and frequency, especially for ATL and PAC2. Strongly prevalent interannual phase-relations between SST indices are generally robust through the integration, with PAC1 fluctuating in rough quadrature with PAC2 and leading ATL (Figure S3). At the interdecadal and multidecadal bands, PAC1-PAC2 phase relations are overall coherent through the integration and indicative of a rough co-phase, while PAC1-ATL phase relations exemplify prominent changes of inter-basin interactions through time (Figure S3).

Thus, for this model and these indices, our inferences about both low-frequency SST variability and inter-basin phasing suffer from considerable uncertainty arising from intrinsic features of the simulated climate. Figure 7 summarizes how such uncertainty reflects variations in the covariance structure of regional SSTs, which is captured by EOF indices. The yellow-to-red lines in Figure 7 are visible when indices calculated over subsequent 500-year periods more strongly differ from respective indices calculated over subsequent 1000-year periods (blue-to-black lines). The green lines illustrate the evolution of full-period indices calculated by projecting the EOFs for the first 500 years of the simulation on the full-period SST data. They are visible when large modifications occur in the covariance structure of SSTs with respect to the initial period. The trajectories of the differently-evaluated indices generally superpose well along the integration, though apparently less satisfying for an EOF analog of ATL (named ATL1, see Figure 7c). For this index differences are prominent between 1000-year, 500-year and projected indices especially during the second millennium of the simulation. However, this is apparently unrelated to a progressively deteriorated skill of the projected index. Rather, the deviations appear to strongly vary between subsequent centennial and multicentennial periods (Figure 7d), meaning that modifications to the covariance structure of regional SSTs are continuous and related to (multi)centennial-scale dynamics. Accordingly, the multicentennial ATL1 pattern remarkably changes through the integration time and shows variable strength of its signature on tropical, mid-latitude and subpolar North Atlantic SSTs (Figure S4).

North Atlantic SST variability is determined by two major contributions: anomalous air-sea energy exchanges linked to changes the large-scale atmospheric circulation and changes in oceanic processes linked to the thermohaline overturning circulation. These can be summarized, respectively, by the AO and AMOC indices (see section 2.2). Temporal variations characterize the correlation of ATL1 with both indices (Figure 7d, dotted lines): the ATL1-AO correlation fluctuates around the value of -0.5 in the first two millennia of the simulation, while it vanishes towards near zero values in the last millennium; similarly, millennial fluctuations characterize the ATL1-AMOC correlation, ranging between values of 0.5 and -0.2. The variable strength of the correlations suggests that the behavior of ATL1 reflects the non-stationary signatures of deep ocean processes and large-scale atmospheric variability on North Atlantic SSTs.

4 Discussion

Our discussion of the results is going to focus on three aspects: i) comparability between simulations and observations, ii) dynamical interpretation, and iii) caveats to our analysis.

4.1 Simulations-observations comparison

We start by noting that the realism of simulated dominant modes of climate variability and of their teleconnections is still questionable in several aspects (Sheffield et al., 2013), as previously exemplified, for instance, for ENSO (Guilyardi et al., 2012; Zou et al., 2014) and for the AMV (Kavvada et al., 2013; Ruiz-Barradas et al., 2013), but possibly less so for the PDO (Sheffield et al., 2013). Common biases in regional SSTs highlight common model deficiencies in the representation of oceanic and coupled ocean-atmosphere processes. Connected distributions of SST biases imply that the effect of remote biases may override good model performance in the simulation of regional processes (Wang et al., 2014).

Furthermore, our analyses compare the ensemble features of simulated unperturbed climates with the observed climate, which was subject to substantial external forcing. However, external forcing can crucially influence internal climate variability through changes in the background climate conditions. For instance, paleo-reconstructions of ENSO indicate an anomalously high ENSO activity in the late twentieth century over the past seven centuries, suggestive of a response to global warming (e.g., Li et al., 2013). External forcing can also amplify and set the phase of decadal variability of North Atlantic SSTs (e.g., Ottera Odd Helge et al., 2010; Booth et al., 2012; Zanchettin et al., 2013). The lack of external forcing in the employed unperturbed simulations may explain part of the found discrepancies between observed and ensemble-simulated features. However, CMIP5 models produce too energetic interannual components of forced climate variability and too weak decadal components in several key regions compared to observations (Ault et al., 2012). Accordingly, ENSO-related variability is overrepresented in historical (forced) MPI-ESM-LR simulations compared to observations while North Atlantic SST variability is under-represented (Tantet and Dijkstra, 2014).

4.2 Dynamical interpretation

Two prevalent features emerge from our ensemble analysis. Firstly, there are a tight inter-basin relationship described by the PAC1-ATL phasing on interannual timescales (Figure 5b) and a similarly strong PAC1-GSST connection (Figure 6a). That is, large-scale Pacific-Atlantic and regional-global interactions are robust among the considered unperturbed climate simulations. The favorable agreement with observations (Figure 2d,e) indicates that simulated internal dynamics capture such interactions notwithstanding uncertainties/deficiencies in the representation of ENSO and of tropical Atlantic variability (for the latter see, e.g., Grodsky et al., 2012). Due to dominant interannual ENSO-like variability, the highlighted inter-basin mechanisms likely include a direct influence of ENSO in the tropical Atlantic sector through its eastward extension (e.g., Wang, 2005; Graf and Zanchettin, 2012) and an indirect influence through the ENSO-induced global changes (e.g., Enfield and Mestas-Nu?ez, 2000). By contrast, Pacific-Atlantic SST relationships independent of ENSO may be hard to be detected.

The second robust feature is the marked convergence of PAC1 and PAC2 on inter- and multi-decadal timescales seen in the ensemble PAC1-PAC2 phase-frequency diagrams (Figure 5a,d). Already both observational PAC indices correlate similarly with the observed PDO index (Section 3.1) and both PAC ensemble-signatures entail a PDO-like horseshoe pattern (Figure 3a,b). A PDO index defined as the first principal component of annual-average SSTs over the extra-tropical North Pacific (120–240°E; 20–50°N) generally strongly correlates with both PAC1 and PAC2 (not shown). This indicates that the PDO is a combination of tropical (PAC1) and extra-tropical (PAC2) processes. The PAC1-PDO connection reflects well-known causal links between ENSO variability and decadal oceanic variability in the extra-tropical North Pacific (e.g., Newman et al., 2003; Vimont, 2005; Di Lorenzo et al., 2010). The PAC2-PDO connection possibly highlights the decadal variability of the Kuroshio-Oyashio Extension (KOE) and of the extra-tropical gyre-scale circulation. Unsatisfactory representation of the observed PAC2 pattern in several simulations (compare Figure 3b) could reflect intrinsic variability of the meridional KOE structure, or, more likely, model deficiencies in (among others) eddy parameterizations and the representation of KOE-related key processes (e.g., Pierce et al., 2001; Taguchi et al., 2007).

Besides these two robust features, our indices lack a clear dominant regional driver of inter- and multi-decadal Pacific and Atlantic SST variability where observational results indicate a decadally-lagged response of the PDO to the AMV (d'Orgeville and Peltier, 2007; Zhang and Delworth, 2007; Wu et al., 2011, compare also the PAC2-ATL multidecadal phasing in Figure 2a). A robust PDO-AMV phasing still does not emerge if the ensemble analysis is repeated for the above-defined PDO index (not shown).

The lack of a clear regional driver could reflect a low signal-to-noise ratio of the propagating signals due to the simulated weak inter- and multi-decadal variability, and/or general model deficiencies regarding processes and dominant mechanism underlying the simulated inter-basin variability. Preliminary results from sensitivity experiments conducted with MPI-ESM-P support the first hypothesis by depicting a robust response of Pacific SSTs to imposed AMV fluctuations, but for amplitudes of the latter substantially larger than those spontaneously generated by the unperturbed model (not shown, manuscript in preparation).

Concerning the latter hypothesis, Wu et al. (2011) discuss a possible mechanism for a decadally-lagged AMV-PDO interaction with a dominant role for a mid-latitude atmospheric connection (Zhang and Delworth, 2007, see also Li et al., 2009); the mid-latitude westerlies over both the Atlantic and Pacific basins shift northward under warm AMV phases due to reduced meridional gradients in mid-latitude North Atlantic SSTs. This initiates a positive feedback loop in the Pacific between the weakened Aleutian low and warm SST anomalies in the KOE region, and vice versa. The ensemble may lack this mechanism due to the general uncertainties associated with the simulated footprint of the AMV within the Atlantic sector (Kavvada et al., 2013). The simulated representation of SSTs in the Gulf Stream regions is especially important for robust atmospheric responses over the Pacific (Li et al., 2009), and a relatively high horizontal resolution — generally higher than that of the presently used models — is necessary for a realistic representation of frontal SST variations influences on atmospheric variability (Hand et al., 2014). Additional deficiencies in the location and variability of the KOE may affect the mid-latitude atmospheric bridge between Pacific and Atlantic oceans (Li et al., 2009; Frankignoul et al., 2011).

Further, the timescale of the PDO response to the Atlantic SST forcing depends on the westward propagation of oceanic Rossby waves excited in the north Pacific by the warm SST anomalies and the positive air-sea feedback in the Pacific (Zhang and Delworth, 2007). Realism and robustness of these features in the employed coupled climate models is unknown. In particular, the eastward advection of KOE SST anomalies by the Kuroshio Current may represent a source of substantial uncertainty affecting our ensemble analysis (Zhang and Delworth, 2007).

Alternatively, the lack of a clear regional driver could result from different inter-basin mechanisms being active/dominant under different circumstances. The MPI-ESM-COSMOS-Mill simulation exemplifies the inherent variability on multicentennial time-scale especially in North Atlantic SSTs. This includes the spatiotemporal evolution of the dominant North Atlantic SST mode and, in particular, of its mid-latitude/subpolar and tropical North Atlantic SST signatures (Figure S4), as well as the varying link with the hemispheric-scale atmospheric circulation and the AMOC (Figure 7). The variety in the relationship between North Atlantic SSTs and the AMOC is similarly depicted by multi-model analyses, with models disagreeing about both phasing and strength of the AMOC-AMV co-variability (Medhaug and Furevik, 2011; Zanchettin et al., 2014). Lohmann et al. (2014) describe the substantial differences and biases that still characterize the representation of the AMOC in coupled climate simulations, with resulting uncertainties including the dominant oceanic processes behind multidecadal AMOC variability.

4.3 Caveats

Our approach refines ensemble cross-correlation analysis by not regarding the full variability but only presenting times and frequencies associated to significant variability through wavelet-based phase-frequency diagrams. Concerns exist whether wavelet cross-spectra, as used here, are suitable for significance testing of the interrelation between two processes (Maraun and Kurths, 2004). The employed surrogate-based tests and basing robustness of detected signals on both, significance and representativeness, increase the confidence in our inferences about prevalent phase relations between paired SST indices.

Using simulations with different length may be questioned since individual simulations have then different weight in generating the ensemble response. We repeated the key analyses on an ensemble comprising the same simulations but with a homogenized length of $\sim$500 years (i.e., using the first 500 years of each simulation at maximum). The homogenized ensemble produces only marginal changes in the phase-frequency diagrams with respect to the full-period analysis, and generally does not change the significance (or lack thereof) of the linkages between regional SST indices, and between them and GSST (results not shown). In particular, results from the homogenized ensemble agree with our inference discussed above that the ensemble lacks robust inter- and multi-decadal inter-basin relations. Consistent results from the single-model analysis further increase confidence in our general conclusions.

5 Conclusions

This study assessed the ensemble representation of internally-generated regional SST variability in a 20-member multi-model ensemble of unperturbed climate simulations from the Coupled Model Intercomparison Project, phase 5 (CMIP5). Ensemble spatial patterns of basin-scale modes of SST variability and ensemble (cross-)wavelet-based phase-frequency diagrams of associated paired indices were used to summarize the ensemble characteristics of inter-basin and regional-to-global SST interactions on a broad range of timescales. The idea was that, if similar underlying physical processes shape regional SST modes in the different simulations within the ensemble, then one can expect the associated ensemble phase-frequency diagrams to highlight the varied but common interdependences among such processes beyond the variability that they express in individual simulations. The multi-model ensemble consistently points towards tropical and North Pacific SSTs being a source of interannual global SST variability. Linearly-independent Pacific indices describing tropical and extra-tropical variability converge toward co-phase at inter- and multi-decadal time scales, indicating that the Pacific Decadal Oscillation is a combination of tropical and extra-tropical processes. Multidecadal fluctuations in the average North Atlantic SSTs generally co-vary with but also often lag global changes, which renders difficult to discern the Atlantic-Multidecadal-Variability signal from the global signal. Whereas individual simulations and/or periods within individual simulations exhibit phase-locked inter- and multi-decadal fluctuations between Pacific and Atlantic modes of SST variability, results are mostly smeared out in the ensemble analysis and produce overall non-robust ensemble signals. We conclude that diversity or non-stationarity of inter- and multi-decadal inter-basin SST relations and of underlying mechanisms are inherent features of unperturbed simulated climates. This constrains the extrapolation of low-frequency phase relations between Pacific and Atlantic SST indices deduced from observations, since they may be a recurrent but non-typical expression of internal climate dynamics. However, the generally weaker amplitude of simulated inter- and multi-decadal variability compared to observations may result in a low signal-to-noise ratio for dominant inter-basin mechanisms. Our results ask for more focused research on the conditions under which phase-locked behavior occurs and on the model-dependence and uncertainties of the underlying mechanism(s).

Acknowledgements. The authors thank two anonymous Reviewers whose comments contributed to substantially improve the study and the paper. The authors also thank Jochem Marotzke, Lorenzo Tomassini and Svante Henriksson for useful comments on early versions of the manuscript. This work was funded by the BMBF (research program MiKlip, FKZ:01LP1158A). We acknowledge the World Climate Research Programme's Working Group on Coupled Modelling and the participating groups for producing and making available the model output. The cross-wavelet software was provided by A. Grinsted (@AGrinsted).

References

Andrews, T., Gregory, J. M., Webb, M. J., and Taylor, K. E.: Forcing, feedbacks and climate sensitivity in CMIP5 coupled atmosphere-ocean climate models, Geophysical Research Letters, 39, L09 712, doi:10.1029/2012GL051607, http://onlinelibrary.wiley.com/doi/10.1029/2012GL051607/abstract, 2012.

Ault, T. R., Cole, J. E., and St. George, S.: The amplitude of decadal to multidecadal variability in precipitation simulated by state-of-the-art climate models, Geophysical Research Letters, 39, L21 705, doi:10.1029/2012GL053424, http://onlinelibrary.wiley.com/doi/10.1029/2012GL053424/abstract, 2012.

Bentsen, M., Bethke, I., Debernard, J. B., Iversen, T., Kirkevåg, A., Seland, Ø., Drange, H., Roelandt, C., Seierstad, I. A., Hoose, C., and Kristjánsson, J. E.: The Norwegian Earth System Model, NorESM1-M – Part 1: Description and basic evaluation of the physical climate, Geosci. Model Dev., 6, 687–720, doi:10.5194/gmd-6-687-2013, http://www.geosci-model-dev.net/6/687/2013/, 2013.

Bhend, J. and Whetton, P.: Consistency of simulated and observed regional changes in temperature, sea level pressure and precipitation, Climatic Change, 118, 799–810, doi:10.1007/s10584-012-0691-2, http://link.springer.com/article/10.1007/s10584-012-0691-2, 2013.

Bi, D., Dix, M., Marsland, S., O'Farrell, S., Rashid, H., Uotila, P., Hirst, A., Kowalczyk, E., Golebiewski, M., Sullivan, A., Yan, H., Hannah, N., Franklin, C., Sun, Z., Vohralik, P., Watterson, I., Zhou, X., Fiedler, R., Collier, M., Ma, Y., Noonan, J., Stevens, L., Uhe, P., Zhu, H., Griffies, S., Hill, R., Harris, C., and Puri, K.: The ACCESS coupled model: description, control climate and evaluation, Aust. Meteorol. Oceanogr. J, 63, 41–64, 2013.

Booth, B. B. B., Dunstone, N. J., Halloran, P. R., Andrews, T., and Bellouin, N.: Aerosols implicated as a prime driver of twentieth-century North Atlantic climate variability, Nature, 484, 228–232, doi:10.1038/nature10946, http://www.nature.com/nature/journal/v484/n7393/full/nature10946.html, 2012.

Bothe, O., Jungclaus, J. H., and Zanchettin, D.: Consistency of the multi-model CMIP5/PMIP3-past1000 ensemble, Clim. Past, 9, 2471–2487, doi:10.5194/cp-9-2471-2013, http://www.clim-past.net/9/2471/2013/, 2013.

Braconnot, P., Harrison, S. P., Kageyama, M., Bartlein, P. J., Masson-Delmotte, V., Abe-Ouchi, A., Otto-Bliesner, B., and Zhao, Y.: Evaluation of climate models using palaeoclimatic data, Nature Climate Change, 2, 417–424, doi:10.1038/nclimate1456, http://www.nature.com/nclimate/journal/v2/n6/full/nclimate1456.html, 2012.

Choi, J., An, S.-I., Kug, J.-S., and Yeh, S.-W.: The role of mean state on changes in El Niño's flavor, Climate Dynamics, 37, 1205–1215, doi:10.1007/s00382-010-0912-1, http://link.springer.com/article/10.1007/s00382-010-0912-1, 2011.

Chylek, P., Li, J., Dubey, M. K., Wang, M., and Lesins, G.: Observed and model simulated 20th century Arctic temperature variability: Canadian Earth System Model CanESM2, Atmos. Chem. Phys. Discuss., 11, 22 893–22 907, doi:10.5194/acpd-11-22893-2011, http://www.atmos-chem-phys-discuss.net/11/22893/2011/, 2011.

Collins, W. J., Bellouin, N., Doutriaux-Boucher, M., Gedney, N., Halloran, P., Hinton, T., Hughes, J., Jones, C. D., Joshi, M., Liddicoat, S., Martin, G., O'Connor, F., Rae, J., Senior, C., Sitch, S., Totterdell, I., Wiltshire, A., and Woodward, S.: Development and evaluation of an Earth-System model – HadGEM2, Geosci. Model Dev., 4, 1051–1075, doi:10.5194/gmd-4-1051-2011, http://www.geosci-model-dev.net/4/1051/2011/, 2011.

Deser, C., Knutti, R., Solomon, S., and Phillips, A. S.: Communication of the role of natural variability in future North American climate, Nature Climate Change, 2, 775–779, doi:10.1038/nclimate1562, http://www.nature.com/nclimate/journal/v2/n11/full/nclimate1562.html, 2012.

Di Lorenzo, E., Cobb, K. M., Furtado, J. C., Schneider, N., Anderson, B. T., Bracco, A., Alexander, M. A., and Vimont, D. J.: Central Pacific El Nino and decadal climate change in the North Pacific Ocean, Nature Geoscience, 3, 762–765, doi:10.1038/ngeo984, http://www.nature.com/ngeo/journal/v3/n11/full/ngeo984.html, 2010.

Donner, L. J., Wyman, B. L., Hemler, R. S., Horowitz, L. W., Ming, Y., Zhao, M., Golaz, J.-C., Ginoux, P., Lin, S.-J., Schwarzkopf, M. D., Austin, J., Alaka, G., Cooke, W. F., Delworth, T. L., Freidenreich, S. M., Gordon, C. T., Griffies, S. M., Held, I. M., Hurlin, W. J., Klein, S. A., Knutson, T. R., Langenhorst, A. R., Lee, H.-C., Lin, Y., Magi, B. I., Malyshev, S. L., Milly, P. C. D., Naik, V., Nath, M. J., Pincus, R., Ploshay, J. J., Ramaswamy, V., Seman, C. J., Shevliakova, E., Sirutis, J. J., Stern, W. F., Stouffer, R. J., Wilson, R. J., Winton, M., Wittenberg, A. T., and Zeng, F.: The Dynamical Core, Physical Parameterizations, and Basic Simulation Characteristics of the Atmospheric Component AM3 of the GFDL Global Coupled Model CM3, Journal of Climate, 24, 3484–3519, doi:10.1175/2011JCLI3955.1, http://journals.ametsoc.org/doi/abs/10.1175/2011JCLI3955.1, 2011.

d'Orgeville, M. and Peltier, W. R.: On the Pacific Decadal Oscillation and the Atlantic Multidecadal Oscillation: Might they be related?, Geophysical Research Letters, 34, L23 705, doi:10.1029/2007GL031584, http://onlinelibrary.wiley.com/doi/10.1029/2007GL031584/abstract, 2007.

Enfield, D. B. and Mestas-Nu?ez, A. M.: Global Modes of ENSO and Non-ENSO Sea Surface Temperature Variability and Their Associations with Climate, in: El Ni%3Fo and the Southern Oscillation, Cambridge University Press, http://dx.doi.org/10.1017/CBO9780511573125.004, 2000.

Enfield, D. B., Mestas-Nuñez, A. M., and Trimble, P. J.: The Atlantic Multidecadal Oscillation and its relation to rainfall and river flows in the continental U.S., Geophysical Research Letters, 28, 2077–2080, doi:10.1029/2000GL012745, http://onlinelibrary.wiley.com/doi/10.1029/2000GL012745/abstract, 2001.

Frankignoul, C., Sennéchael, N., Kwon, Y.-O., and Alexander, M. A.: Influence of the Meridional Shifts of the Kuroshio and the Oyashio Extensions on the Atmospheric Circulation, Journal of Climate, 24, 762–777, doi:10.1175/2010JCLI3731.1, http://journals.ametsoc.org/doi/abs/10.1175/2010JCLI3731.1, 2011.

Fritsch, J. M., Hilliker, J., Ross, J., and Vislocky, R. L.: Model Consensus, Weather and Forecasting, 15, 571–582, doi:10.1175/1520-0434(2000)015<0571:MC>2.0.CO;2, http://journals.ametsoc.org/doi/abs/10.1175/1520-0434(2000)015%3C0571:MC%3E2.0.CO%3B2, 2000.

Ge, Z.: Significance tests for the wavelet cross spectrum and wavelet linear coherence, Ann. Geophys., 26, 3819–3829, doi:10.5194/angeo-26-3819-2008, http://www.ann-geophys.net/26/3819/2008/, 2008.

Gent, P. R., Danabasoglu, G., Donner, L. J., Holland, M. M., Hunke, E. C., Jayne, S. R., Lawrence, D. M., Neale, R. B., Rasch, P. J., Vertenstein, M., Worley, P. H., Yang, Z.-L., and Zhang, M.: The Community Climate System Model Version 4, Journal of Climate, 24, 4973–4991, doi:10.1175/2011JCLI4083.1, http://journals.ametsoc.org/doi/abs/10.1175/2011JCLI4083.1, 2011.

Giorgetta, M. A., Jungclaus, J., Reick, C. H., Legutke, S., Bader, J., Böttinger, M., Brovkin, V., Crueger, T., Esch, M., Fieg, K., Glushak, K., Gayler, V., Haak, H., Hollweg, H.-D., Ilyina, T., Kinne, S., Kornblueh, L., Matei, D., Mauritsen, T., Mikolajewicz, U., Mueller, W., Notz, D., Pithan, F., Raddatz, T., Rast, S., Redler, R., Roeckner, E., Schmidt, H., Schnur, R., Segschneider, J., Six, K. D., Stockhause, M., Timmreck, C., Wegner, J., Widmann, H., Wieners, K.-H., Claussen, M., Marotzke, J., and Stevens, B.: Climate and carbon cycle changes from 1850 to 2100 in MPI-ESM simulations for the Coupled Model Intercomparison Project phase 5, Journal of Advances in Modeling Earth Systems, 5, 572–597, doi:10.1002/jame.20038, http://onlinelibrary.wiley.com/doi/10.1002/jame.20038/abstract, 2013.

Graf, H.-F. and Zanchettin, D.: Central Pacific El Niño, the "subtropical bridge," and Eurasian climate, Journal of Geophysical Research: Atmospheres, 117, D01 102, doi:10.1029/2011JD016493, http://onlinelibrary.wiley.com/doi/10.1029/2011JD016493/abstract, 2012.

Griffies, S. M. and Bryan, K.: A predictability study of simulated North Atlantic multidecadal variability, Climate Dynamics, 13, 459–487, doi:10.1007/s003820050177, http://link.springer.com/article/10.1007/s003820050177, 1997.

Griffies, S. M., Winton, M., Donner, L. J., Horowitz, L. W., Downes, S. M., Farneti, R., Gnanadesikan, A., Hurlin, W. J., Lee, H.-C., Liang, Z., Palter, J. B., Samuels, B. L., Wittenberg, A. T., Wyman, B. L., Yin, J., and Zadeh, N.: The GFDL CM3 Coupled Climate Model: Characteristics of the Ocean and Sea Ice Simulations, Journal of Climate, 24, 3520–3544, doi:10.1175/2011JCLI3964.1, http://journals.ametsoc.org/doi/abs/10.1175/2011JCLI3964.1, 2011.

Grinsted, A., Moore, J. C., and Jevrejeva, S.: Application of the cross wavelet transform and wavelet coherence to geophysical time series, Nonlin. Processes Geophys., 11, 561–566, doi:10.5194/npg-11-561-2004, http://www.nonlin-processes-geophys.net/11/561/2004/, 2004.

Grodsky, S. A., Carton, J. A., Nigam, S., and Okumura, Y. M.: Tropical Atlantic Biases in CCSM4, Journal of Climate, 25, 3684–3701, doi:10.1175/JCLI-D-11-00315.1, http://journals.ametsoc.org/doi/abs/10.1175/JCLI-D-11-00315.1, 2012.

Grossmann, I. and Klotzbach, P. J.: A review of North Atlantic modes of natural variability and their driving mechanisms, Journal of Geophysical Research: Atmospheres, 114, D24 107, doi:10.1029/2009JD012728, http://onlinelibrary.wiley.com/doi/10.1029/2009JD012728/abstract, 2009.

Guilyardi, E., Bellenger, H., Collins, M., Ferrett, S., Cai, W., and Wittenberg, A.: A first look at ENSO in CMIP5, Clivar Exchanges, 17, 29–32, 2012.

Hand, R., Keenlyside, N., Omrani, N.-E., and Latif, M.: Simulated response to inter-annual SST variations in the Gulf Stream region, Climate Dynamics, 42, 715–731, doi:10.1007/s00382-013-1715-y, http://link.springer.com/article/10.1007/s00382-013-1715-y, 2014.

Joetzjer, E., Douville, H., Delire, C., and Ciais, P.: Present-day and future Amazonian precipitation in global climate models: CMIP5 versus CMIP3, Climate Dynamics, 41, 2921–2936, doi:10.1007/s00382-012-1644-1, http://link.springer.com/article/10.1007/s00382-012-1644-1, 2013.

Jones, C. D., Hughes, J. K., Bellouin, N., Hardiman, S. C., Jones, G. S., Knight, J., Liddicoat, S., O'Connor, F. M., Andres, R. J., Bell, C., Boo, K.-O., Bozzo, A., Butchart, N., Cadule, P., Corbin, K. D., Doutriaux-Boucher, M., Friedlingstein, P., Gornall, J., Gray, L., Halloran, P. R., Hurtt, G., Ingram, W. J., Lamarque, J.-F., Law, R. M., Meinshausen, M., Osprey, S., Palin, E. J., Parsons Chini, L., Raddatz, T., Sanderson, M. G., Sellar, A. A., Schurer, A., Valdes, P., Wood, N., Woodward, S., Yoshioka, M., and Zerroukat, M.: The HadGEM2-ES implementation of CMIP5 centennial simulations, Geosci. Model Dev., 4, 543–570, doi:10.5194/gmd-4-543-2011, http://www.geosci-model-dev.net/4/543/2011/, 2011.

Jungclaus, J. H., Lorenz, S. J., Timmreck, C., Reick, C. H., Brovkin, V., Six, K., Segschneider, J., Giorgetta, M. A., Crowley, T. J., Pongratz, J., Krivova, N. A., Vieira, L. E., Solanki, S. K., Klocke, D., Botzet, M., Esch, M., Gayler, V., Haak, H., Raddatz, T. J., Roeckner, E., Schnur, R., Widmann, H., Claussen, M., Stevens, B., and Marotzke, J.: Climate and carbon-cycle variability over the last millennium, Clim. Past, 6, 723–737, doi:10.5194/cp-6-723-2010, http://www.clim-past.net/6/723/2010/, 2010.

Jungclaus, J. H., Fischer, N., Haak, H., Lohmann, K., Marotzke, J., Matei, D., Mikolajewicz, U., Notz, D., and von Storch, J. S.: Characteristics of the ocean simulations in the Max Planck Institute Ocean Model (MPIOM) the ocean component of the MPI-Earth system model, Journal of Advances in Modeling Earth Systems, 5, 422–446, doi:10.1002/jame.20023, http://onlinelibrary.wiley.com/doi/10.1002/jame.20023/abstract, 2013.

Kavvada, A., Ruiz-Barradas, A., and Nigam, S.: AMO's structure and climate footprint in observations and IPCC AR5 climate simulations, Climate Dynamics, 41, 1345–1364, doi:10.1007/s00382-013-1712-1, http://link.springer.com/article/10.1007/s00382-013-1712-1, 2013.

Knight, J. R.: The Atlantic Multidecadal Oscillation Inferred from the Forced Climate Response in Coupled General Circulation Models, Journal of Climate, 22, 1610–1625, doi:10.1175/2008JCLI2628.1, http://journals.ametsoc.org/doi/abs/10.1175/2008JCLI2628.1, 2009.

Knutti, R., Abramowitz, G., Collins, M., Eyring, V., Gleckler, P., Hewitson, B., and Mearns, L.: Good practice guidance paper on assessing and combining multi model climate projections, Report, IPCC Working Group I Technical Support Unit, University of Bern, Bern, Switzerland, 2010.

Li, C., Wu, L., Wang, Q., Qu, L., and Zhang, L.: An intimate coupling of ocean–atmospheric interaction over the extratropical North Atlantic and Pacific, Climate Dynamics, 32, 753–765, doi:10.1007/s00382-009-0529-4, http://link.springer.com/article/10.1007/s00382-009-0529-4, 2009.

Li, J., Xie, S.-P., Cook, E. R., Morales, M. S., Christie, D. A., Johnson, N. C., Chen, F., D'Arrigo, R., Fowler, A. M., Gou, X., and Fang, K.: El Nino modulations over the past seven centuries, Nature Climate Change, 3, 822–826, doi:10.1038/nclimate1936, http://www.nature.com/nclimate/journal/v3/n9/full/nclimate1936.html, 2013.

Liu, Z.: Dynamics of Interdecadal Climate Variability: A Historical Perspective*, Journal of Climate, 25, 1963–1995, doi:10.1175/2011JCLI3980.1, http://journals.ametsoc.org/doi/abs/10.1175/2011JCLI3980.1, 2012.

Lohmann, K., Jungclaus, J. H., Matei, D., Mignot, J., Menary, M., Langehaug, H. R., Ba, J., Gao, Y., Otterå, O. H., Park, W., and Lorenz, S.: The role of subpolar deep water formation and Nordic Seas overflows in simulated multidecadal variability of the Atlantic meridional overturning circulation, Ocean Sci., 10, 227–241, doi:10.5194/os-10-227-2014, http://www.ocean-sci.net/10/227/2014/, 2014.

Long, M. C., Lindsay, K., Peacock, S., Moore, J. K., and Doney, S. C.: Twentieth-Century Oceanic Carbon Uptake and Storage in CESM1(BGC)*, Journal of Climate, 26, 6775–6800, doi:10.1175/JCLI-D-12-00184.1, http://journals.ametsoc.org/doi/abs/10.1175/JCLI-D-12-00184.1, 2013.

Mantua, N. J., Hare, S. R., Zhang, Y., Wallace, J. M., and Francis, R. C.: A Pacific Interdecadal Climate Oscillation with Impacts on Salmon Production, Bulletin of the American Meteorological Society, 78, 1069–1079, doi:10.1175/1520-0477(1997)078<1069:APICOW>2.0.CO;2, http://journals.ametsoc.org/doi/abs/10.1175/1520-0477(1997)078%3C1069%3AAPICOW%3E2.0.CO%3B2, 1997.

Maraun, D. and Kurths, J.: Cross wavelet analysis: significance testing and pitfalls, Nonlin. Processes Geophys., 11, 505–514, doi:10.5194/npg-11-505-2004, http://www.nonlin-processes-geophys.net/11/505/2004/, 2004.

Medhaug, I. and Furevik, T.: North Atlantic 20th century multidecadal variability in coupled climate models: sea surface temperature and ocean overturning circulation, Ocean Sci., 7, 389–404, doi:10.5194/os-7-389-2011, http://www.ocean-sci.net/7/389/2011/, 2011.

Müller, W. A. and Roeckner, E.: ENSO teleconnections in projections of future climate in ECHAM5/MPI-OM, Climate Dynamics, 31, 533–549, doi:10.1007/s00382-007-0357-3, http://link.springer.com/article/10.1007/s00382-007-0357-3, 2008.

Newman, M., Compo, G. P., and Alexander, M. A.: ENSO-Forced Variability of the Pacific Decadal Oscillation, Journal of Climate, 16, 3853–3857, doi:10.1175/1520-0442(2003)016<3853:EVOTPD>2.0.CO;2, http://journals.ametsoc.org/doi/abs/10.1175/1520-0442(2003)016%3C3853:EVOTPD%3E2.0.CO;2, 2003.

Ottera Odd Helge, Bentsen Mats, Drange Helge, and Suo Lingling: External forcing as a metronome for Atlantic multidecadal variability, Nature Geosci, 3, 688–694, doi:http://dx.doi.org/10.1038/ngeo955, http://www.nature.com/ngeo/journal/v3/n10/abs/ngeo955.html#supplementary-information, 10.1038/ngeo955, 2010.

Park, W. and Latif, M.: Pacific and Atlantic multidecadal variability in the Kiel Climate Model, Geophysical Research Letters, 37, L24 702, doi:10.1029/2010GL045560, http://onlinelibrary.wiley.com/doi/10.1029/2010GL045560/abstract, 2010.

Phipps, S. J., Rotstayn, L. D., Gordon, H. B., Roberts, J. L., Hirst, A. C., and Budd, W. F.: The CSIRO Mk3L climate system model version 1.0 – Part 1: Description and evaluation, Geosci. Model Dev., 4, 483–509, doi:10.5194/gmd-4-483-2011, http://www.geosci-model-dev.net/4/483/2011/, 2011.

Phipps, S. J., Rotstayn, L. D., Gordon, H. B., Roberts, J. L., Hirst, A. C., and Budd, W. F.: The CSIRO Mk3L climate system model version 1.0 – Part 2: Response to external forcings, Geosci. Model Dev., 5, 649–682, doi:10.5194/gmd-5-649-2012, http://www.geosci-model-dev.net/5/649/2012/, 2012.

Pierce, D. W., Barnett, T. P., Schneider, N., Saravanan, R., Dommenget, D., and Latif, M.: The role of ocean dynamics in producing decadal climate variability in the North Pacific, Climate Dynamics, 18, 51–70, doi:10.1007/s003820100158, http://link.springer.com/article/10.1007/s003820100158, 2001.

Rayner, N. A., Parker, D. E., Horton, E. B., Folland, C. K., Alexander, L. V., Rowell, D. P., Kent, E. C., and Kaplan, A.: Global analyses of sea surface temperature, sea ice, and night marine air temperature since the late nineteenth century, Journal of Geophysical Research: Atmospheres, 108, 4407, doi:10.1029/2002JD002670, http://onlinelibrary.wiley.com/doi/10.1029/2002JD002670/abstract, 2003.

Rotstayn, L. D., Jeffrey, S. J., Collier, M. A., Dravitzki, S. M., Hirst, A. C., Syktus, J. I., and Wong, K. K.: Aerosol- and greenhouse gas-induced changes in summer rainfall and circulation in the Australasian region: a study using single-forcing climate simulations, Atmos. Chem. Phys., 12, 6377–6404, doi:10.5194/acp-12-6377-2012, http://www.atmos-chem-phys.net/12/6377/2012/, 2012.

Ruiz-Barradas, A., Nigam, S., and Kavvada, A.: The Atlantic Multidecadal Oscillation in twentieth century climate simulations: uneven progress from CMIP3 to CMIP5, Climate Dynamics, 41, 3301–3315, doi:10.1007/s00382-013-1810-0, http://link.springer.com/article/10.1007/s00382-013-1810-0, 2013.

Russell, A. M. and Gnanadesikan, A.: Understanding Multidecadal Variability in ENSO Amplitude, Journal of Climate, 27, 4037–4051, doi:10.1175/JCLI-D-13-00147.1, http://journals.ametsoc.org/doi/abs/10.1175/JCLI-D-13-00147.1, 2014.

Sheffield, J., Camargo, S. J., Fu, R., Hu, Q., Jiang, X., Johnson, N., Karnauskas, K. B., Kim, S. T., Kinter, J., Kumar, S., Langenbrunner, B., Maloney, E., Mariotti, A., Meyerson, J. E., Neelin, J. D., Nigam, S., Pan, Z., Ruiz-Barradas, A., Seager, R., Serra, Y. L., Sun, D.-Z., Wang, C., Xie, S.-P., Yu, J.-Y., Zhang, T., and Zhao, M.: North American Climate in CMIP5 Experiments. Part II: Evaluation of Historical Simulations of Intraseasonal to Decadal Variability, Journal of Climate, 26, 9247–9290, doi:10.1175/JCLI-D-12-00593.1, http://journals.ametsoc.org/doi/abs/10.1175/JCLI-D-12-00593.1, 2013.

Taguchi, B., Xie, S.-P., Schneider, N., Nonaka, M., Sasaki, H., and Sasai, Y.: Decadal Variability of the Kuroshio Extension: Observations and an Eddy-Resolving Model Hindcast*, Journal of Climate, 20, 2357–2377, doi:10.1175/JCLI4142.1, http://journals.ametsoc.org/doi/abs/10.1175/JCLI4142.1, 2007.

Tantet, A. and Dijkstra, H. A.: An interaction network perspective on the relation between patterns of sea surface temperature variability and global mean surface temperature, Earth Syst. Dynam., 5, 1–14, doi:10.5194/esd-5-1-2014, http://www.earth-syst-dynam.net/5/1/2014/, 2014.

Taylor, K. E., Stouffer, R. J., and Meehl, G. A.: An Overview of CMIP5 and the Experiment Design, Bulletin of the American Meteorological Society, 93, 485–498, doi:10.1175/BAMS-D-11-00094.1, http://journals.ametsoc.org/doi/abs/10.1175/BAMS-D-11-00094.1, 2011.

van Oldenborgh, G. J., Reyes, F. J. D., Drijfhout, S. S., and Hawkins, E.: Reliability of regional climate model trends, Environmental Research Letters, 8, 014 055, doi:10.1088/1748-9326/8/1/014055, http://iopscience.iop.org/1748-9326/8/1/014055, 2013.

Vimont, D. J.: The Contribution of the Interannual ENSO Cycle to the Spatial Pattern of Decadal ENSO-Like Variability*, Journal of Climate, 18, 2080–2092, doi:10.1175/JCLI3365.1, http://journals.ametsoc.org/doi/abs/10.1175/JCLI3365.1, 2005.

Voldoire, A., Sanchez-Gomez, E., Mélia, D. S. y., Decharme, B., Cassou, C., Sénési, S., Valcke, S., Beau, I., Alias, A., Chevallier, M., Déqué, M., Deshayes, J., Douville, H., Fernandez, E., Madec, G., Maisonnave, E., Moine, M.-P., Planton, S., Saint-Martin, D., Szopa, S., Tyteca, S., Alkama, R., Belamari, S., Braun, A., Coquart, L., and Chauvin, F.: The CNRM-CM5.1 global climate model: description and basic evaluation, Climate Dynamics, 40, 2091–2121, doi:10.1007/s00382-011-1259-y, http://link.springer.com/article/10.1007/s00382-011-1259-y, 2012.

Wang, C.: ENSO, Atlantic Climate Variability, and the Walker and Hadley Circulations, in: The Hadley Circulation: Present, Past and Future, edited by Diaz, H. F. and Bradley, R. S., no. 21 in Advances in Global Change Research, pp. 173–202, Springer Netherlands, http://link.springer.com/chapter/10.1007/978-1-4020-2944-8_7, 2005.

Wang, C., Zhang, L., Lee, S.-K., Wu, L., and Mechoso, C. R.: A global perspective on CMIP5 climate model biases, Nature Climate Change, 4, 201–205, doi:10.1038/nclimate2118, http://www.nature.com/nclimate/journal/v4/n3/full/nclimate2118.html, 2014.

Watanabe, M., Suzuki, T., O'ishi, R., Komuro, Y., Watanabe, S., Emori, S., Takemura, T., Chikira, M., Ogura, T., Sekiguchi, M., Takata, K., Yamazaki, D., Yokohata, T., Nozawa, T., Hasumi, H., Tatebe, H., and Kimoto, M.: Improved Climate Simulation by MIROC5: Mean States, Variability, and Climate Sensitivity, Journal of Climate, 23, 6312–6335, doi:10.1175/2010JCLI3679.1, http://journals.ametsoc.org/doi/full/10.1175/2010JCLI3679.1, 2010.

Wu, S., Liu, Z., Zhang, R., and Delworth, T. L.: On the observed relationship between the Pacific Decadal Oscillation and the Atlantic Multi-decadal Oscillation, Journal of Oceanography, 67, 27–35, doi:10.1007/s10872-011-0003-x, http://link.springer.com/article/10.1007/s10872-011-0003-x, 2011.

Yoshimori, M., Raible, C. C., Stocker, T. F., and Renold, M.: Simulated decadal oscillations of the Atlantic meridional overturning circulation in a cold climate state, Climate Dynamics, 34, 101–121, doi:10.1007/s00382-009-0540-9, http://link.springer.com/article/10.1007/s00382-009-0540-9, 2010.

Zanchettin, D., Rubino, A., Traverso, P., and Tomasino, M.: Impact of variations in solar activity on hydrological decadal patterns in northern Italy, Journal of Geophysical Research: Atmospheres, 113, D12 102, doi:10.1029/2007JD009157, http://onlinelibrary.wiley.com/doi/10.1029/2007JD009157/abstract, 2008.

Zanchettin, D., Rubino, A., and Jungclaus, J. H.: Intermittent multidecadal-to-centennial fluctuations dominate global temperature evolution over the last millennium, Geophysical Research Letters, 37, L14 702, doi:10.1029/2010GL043717, http://onlinelibrary.wiley.com/doi/10.1029/2010GL043717/abstract, 2010.

Zanchettin, D., Rubino, A., Matei, D., Bothe, O., and Jungclaus, J. H.: Multidecadal-to-centennial SST variability in the MPI-ESM simulation ensemble for the last millennium, Climate Dynamics, 40, 1301–1318, doi:10.1007/s00382-012-1361-9, http://link.springer.com/article/10.1007/s00382-012-1361-9, 2013.

Zanchettin, D., Bothe, O., Müller, W., Bader, J., and Jungclaus, J. H.: Different flavors of the Atlantic Multidecadal Variability, Climate Dynamics, 42, 381–399, doi:10.1007/s00382-013-1669-0, http://link.springer.com/article/10.1007/s00382-013-1669-0, 2014.

Zhang, R. and Delworth, T. L.: Impact of the Atlantic Multidecadal Oscillation on North Pacific climate variability, Geophysical Research Letters, 34, L23 708, doi:10.1029/2007GL031601, http://onlinelibrary.wiley.com/doi/10.1029/2007GL031601/abstract, 2007.

Zhang, R., Delworth, T. L., Sutton, R., Hodson, D. L. R., Dixon, K. W., Held, I. M., Kushnir, Y., Marshall, J., Ming, Y., Msadek, R., Robson, J., Rosati, A. J., Ting, M., and Vecchi, G. A.: Have Aerosols Caused the Observed Atlantic Multidecadal Variability?, Journal of the Atmospheric Sciences, 70, 1135–1144, doi:10.1175/JAS-D-12-0331.1, http://journals.ametsoc.org/doi/abs/10.1175/JAS-D-12-0331.1, 2013.

Zou, Y., Yu, J.-Y., Lee, T., Lu, M.-M., and Kim, S. T.: CMIP5 model simulations of the impacts of the two types of El Niño on the U.S. winter temperature, Journal of Geophysical Research: Atmospheres, 119, 3076–3092, doi:10.1002/2013JD021064, http://dx.doi.org/10.1002/2013JD021064, 2014.

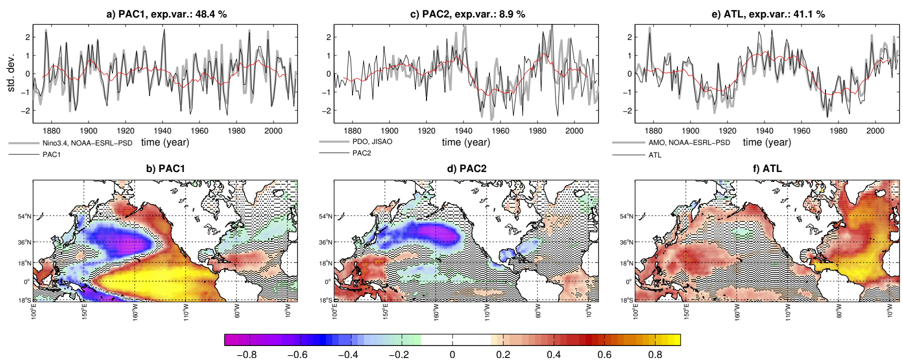

Figure 1. Standardized time series of selected indices **(a,c,e)** and associated regression patterns of standardized North Pacific and North Atlantic SSTs **(b,d,f)** calculated from locally detrended (quadratic fit) HadISST data. Regressions are therefore unitless. Black (red) lines in panels a,c,e are annual-average (smoothed, 11-year running average) time series. Grey lines are reference standardized, annual-averaged indices from known SST modes. Dots in panels **b,d,f** indicate grid-points where the regression is not significant at 95% confidence level accounting for autocorrelation.

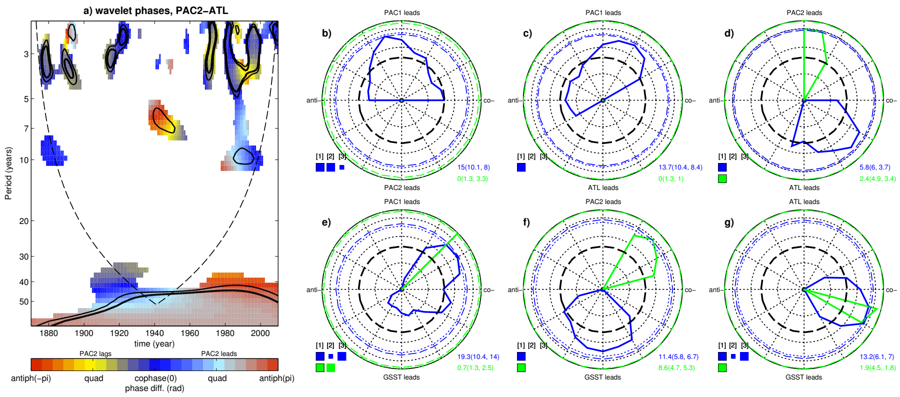

Figure 2. Panel **a**: filled contours: observed PAC2-ATL cross-wavelet phase differences for regions of the cross-wavelet spectrum significant at 75% confidence; continuous black lines: regions of the spectrum significant at 90% (thin) and 95% (thick) confidence; dashed line: cone of influence, delimiting the region of the spectrum where border effects occur. Panels **b–g**: phase-frequency diagrams describing the relative occurrence (frequency) of phase relations between pairs of observed SST indices and GSST for different timescales (blue: interannual; green: interdecadal). Dashed (dotted) colored lines are 95% confidence levels evaluated by method 2 (method 3) described in section 2.2. The extent of significant regions for the different timescales is reported, in percent, by the numbers on the bottom right of each panel (in brackets are the mean values for the random realizations for methods 2 and 3 described in section 2.2). Black thick dashed circle: expected uniform distribution (i.e., if relative occurrence would be the same for all considered phase bands). Small, large and bracketed squares on the bottom left of each panel indicate, respectively, rejection of the null hypothesis with 90%, 95% and 99% confidence according to the three performed tests (numbered on the top). Grid is drawn at $\pi/6$ and at frequency intervals of 0.01, 0.1 and 0.5 (on a log_2 scale in the range $[01]$). In all panels, labels at quadrature phases are according to an expected co-phase. All indices are calculated based on locally detrended (quadratic fit) HadISST data as for Figure 1.

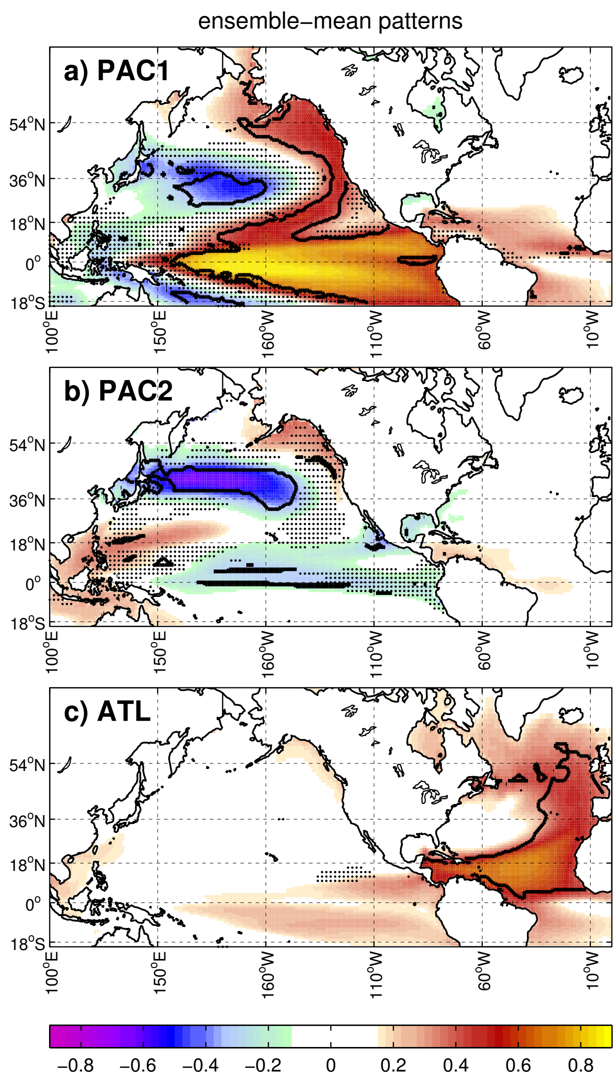

Figure 3. Ensemble-mean regression patterns of standardized tropical-North Pacific and North Atlantic SSTs on selected indices. Regression statistics (unitless) for individual simulations were regridded to a $1^\circ \times 1^\circ$ regular grid. Thick line contours indicate locations where the regression is significant at 95% confidence level in all simulations; dots indicate locations where the ensemble standard deviation of local regression is larger than 0.2. CSIRO-Mk3-6-0/-Mk3L-1-2, FIO-ESM, GISS-E2-H/-R and MIROC5 were excluded in the ensemble analysis for panel **b**.

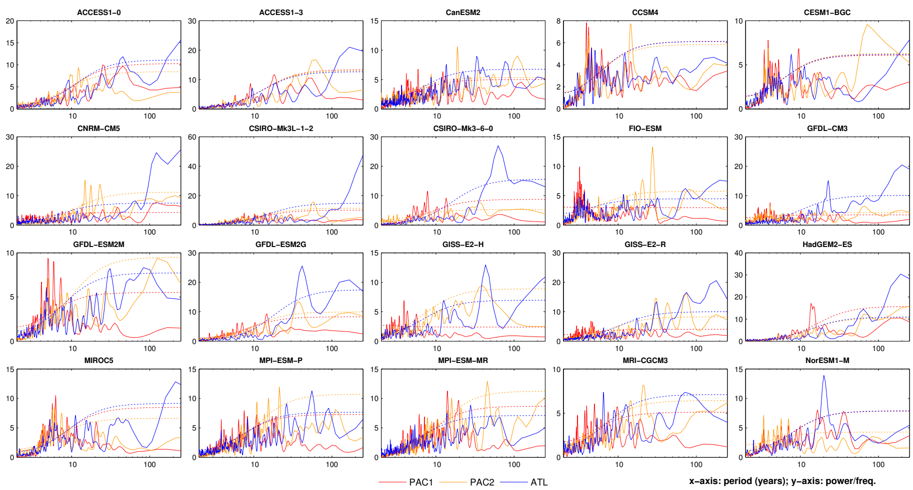

Figure 4. Spectral density (via smoothing of periodogram with Hamming window) of SST indices for individual simulations. The dashed lines individuate the corresponding 95% confidence levels against red noise, calculated for a lag-1 autoregressive process fitted to the data.

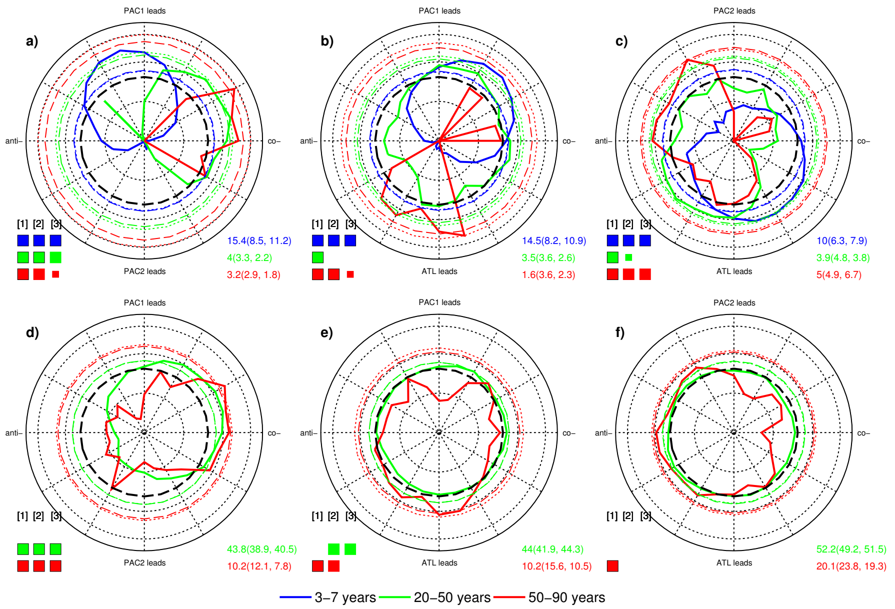

Figure 5. Ensemble phase-frequency diagrams describing phase relations between pairs of SST indices for different timescales (blue: interannual; green: interdecadal; red: multidecadal) for annual **(panels a-c)** and decadally-smoothed **(d-f)** indices. Only significant regions of the cross-wavelet spectrum are retained for the calculation of the diagrams. The extent of significant regions for the different timescales is reported, in percent, by the numbers on the bottom right of each panel (in brackets are the mean values for the random realizations for methods 2 and 3 described in section 2.2). Dashed and dotted colored lines are 95% confidence levels evaluated by methods 2 and 3, respectively. Black thick dashed circle: expected uniform distribution. Small, large and bracketed squares on the bottom left of each panel indicate, respectively, rejection of the null hypothesis with 90%, 95% and 99% confidence according to the three performed tests (numbered on the top). Grid is drawn at $\pi/6$ and at frequency intervals of 0.01, 0.1 and 0.5 (on a log_2 scale in the range $[0, 1]$). Labels at quadrature phases are according to an expected co-phase. CSIRO-Mk3-6-0/-Mk3L-1-2, FIO-ESM, GISS-E2-H/-R and MIROC5 were excluded in the ensemble analysis for panels **a**, **c**, **d** and **f**.

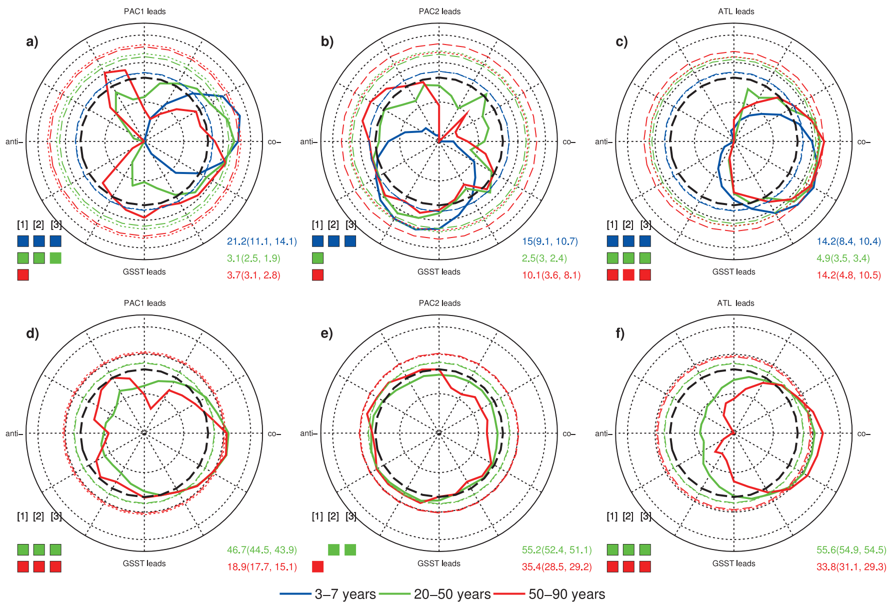

Figure 6. Same as Figure 5, but for the phase relation between SST indices and global-average SST (GSST). GSST data were detrended before analysis (see Table 1). CSIRO-Mk3-6-0/-Mk3L-1-2, FIO-ESM, GISS-E2-H/-R and MIROC5 were excluded in the ensemble analysis for panels **b** and **e**.

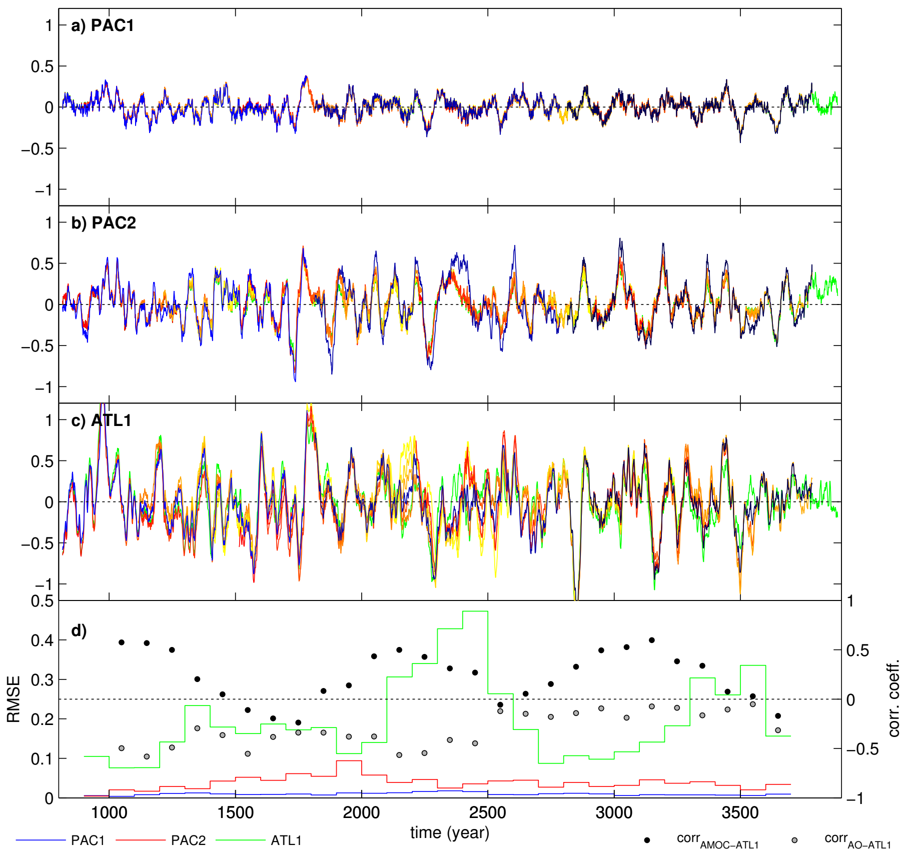

Figure 7. Assessment of uncertainty in EOF-based regional SST indices for the COSMOS-Mill simulation. Temporal evolution of **(a)** PAC1, **(b)** PAC2, and **(c)** ATL1, the EOF analog of ATL (defined as to have generally positive correlations in the tropical North Atlantic). Blue to black lines: index calculated for three consecutive 1000-year slices of the integration; yellow to red lines: index calculated for 500-year slices of the integration paced at 100-year intervals; green: full-period index calculated by projecting the EOF for the first 500 years of the integration on the full-period SST data. **(d)** Left/Continuous lines: Root Mean Squared Error (RMSE) of ensemble 500-year indices versus the projected index averaged over consecutive 100-year periods of the integration (for each 100-year period, the plotted RMSE is the average of the RMSE of the overlapping 500-year indices). Right/Dots: 500-year running-period correlations of the projected ATL1 index with the AMOC index (black) and the full-period AO index (gray). Data are smoothed with a 31-year moving average filter before the analysis.

Table 1. Simulations considered in this study. The employed pre-CMIP5 simulation is indicated in italics. Columns, from left: model; atmospheric and oceanic components (with resolution in brackets); name of the simulation following the notation in the CMIP5 repository, considered period and subtracted long-term trend component (order of the polynomial fit in square brackets); references/sources of information. Names of models and simulations follow the acronyms adopted in the CMIP5 repository.

Model	Atm/Oce components	Simulation (reference period) [trend]	Reference / Sources
ACCESS1-0	UM 7.3-HadGEM2 (N95L38) /MOM4p1 (1° zonal, L50)+ CICE4.1	piControl_r1i1p1 (300-799) [1]	Bi et al. (2013)
ACCESS1-3	UM 7.3-HadGEM3 (N96L38) /MOM4p1 (1° zonal, L50)+ CICE4.1	piControl_r1i1p1 (250-749) [0]	Bi et al. (2013)
CanESM2	CanCM4 with CTEM	piControl_r1i1p1 (2015-3010) [1]	Chylek et al. (2011)
CCSM4	CAM4 (1.25° ×0.9°L26)/Parallel Ocean Model 2 (1°L60)	piControl_r1i1p1 (800-1300) [1]	Gent et al. (2011)
CESM1-BGC	CAM4 (1.25° ×0.9°L26)/Parallel Ocean Model 2 (1°L60), with sea-ice model CICE4	piControl_r1i1p1 (101-600) [0]	Long et al. (2013)
CNRM-CM5	ARPEGE-Climat 5.2 (T127, L31)/ NEMO 3.2 (ORCA1°)	piControl_r1i1p1 (1850-2699) [2]	Voldoire et al. (2012)
COSMOS-Mill	ECHAM5 (T31L19)/MPIOM(GR30L40)	mil0001 (800-3900) [0]	Jungclaus et al. (2010)
CSIRO-Mk3L-1-2	64×56×L18/128×112×L21	piControl_r1i1p1 (1-1000) [1]	Phipps et al. (2011, 2012)
CSIRO-Mk3-6-0	192×96×L18 /192×192×L31	piControl_r1i1p1 (1-500) [1]	Rotstayn et al. (2012)
FiO-ESM	CAM 3.5 (128×64 L26)/ POP 2.0 (320×384 L40)	piControl_r1i1p1 (401-1200) [3]	
GFDL-CM3	AM3/MOM	piControl_r1i1p1 (1-800) [1]	Donner et al. (2011); Griffies et al. (2011)
GFDL-ESM2G	AM3/MOM4.1	piControl_r1i1p1 (1-500) [0]	www.gfdl.noaa.gov/earth-system-model
GFDL-ESM2M	AM3/GOLD	piControl_r1i1p1 (1-500) [1]	www.gfdl.noaa.gov/earth-system-model
GISS-E2-H	ModelE(2° × 2.5°L40)/Hycom(Ĩ° × 1° × L26)	piControl_r1i1p3 (2590-3020) [1]	http://data.giss.nasa.gov/modelE/ar5/
GISS-E2-R	ModelE(2° × 2.5°L40)/Russell (1° × 1.25°L32)	piControl_r1i1p141 (1112-2012) [1]	http://data.giss.nasa.gov/modelE/ar5/
HadGEM2-ES	Atm: N96(1.25° × 1.875°)/L38/oce:1-degree horizontal resolution (increasing to 1/3 degree at the equator)	piControl_r1i1p1 (1859-2435) [1]	Collins et al. (2011); Jones et al. (2011)
MIROC5	FRCGC (L40)/ COCO4.5 (1.48° zonal, L49)	piControl_r1i1p1 (2030-2669) [2]	Watanabe et al. (2010)
MPI-ESM-MR	ECHAM6 (T63L95)/MPIOM(TP04L40)	piControl_r1i1p1-MR (1850-2849) [0]	Giorgetta et al. (2013); Jungclaus et al. (2013)
MPI-ESM-P	ECHAM6 (T63L47)/MPIOM(GR15L40)	piControl_r1i1p1-P (1850-2849) [0]	Giorgetta et al. (2013); Jungclaus et al. (2013)
MRI-CGCM3	MRI-AGCM3 (T159 L48)/ MRI.COM3 (tripolar, 0.5° × 1° L51)	piControl_r1i1p1 (1851-2350) [1]	www.mri-jma.go.jp/Publish/Technical/DATA/VOL_64/tec_rep_mri_64.pdf
NorESM1-M	CAM 4.1.08 (1.9° ×2.5°) MICOM (1.125° at equator)	piControl_r1i1p1 (700-1200) [1]	Bentsen et al. (2013)